INTEGRATION AND IDENTIFICATION OF ACTIVE VIBRATION CONTROL SYSTEM FOR SMART FLEXIBLE STRUCTURES

Nemanja D. Zorić

Faculty of Mechanical Engineering,
The University of Belgrade, Kraljice Marije 16, 11120 Belgrade 35
e-mail: nzoric@mas.bg.ac.rs

Abstract:

The design process of a smart structure for active vibration control involves integration of actuators, sensors, signal conditioning systems and controllers into a flexible structure. These components should be chosen and integrated in such way that obtained smart structure presents functional system. This paper describes procedure of selection and integration of piezoelectric actuators, sensors, signal conditioning system and piezoelectric actuator driver into cantilever aluminum beam in order to achieve desired performances for active vibration control. Signal conditioning from strain gauges and piezoelectric sensors is explained. Also, experimental system identification is performed. According to the experimental data, integer order and fractional-order transfer functions are obtained in order to show if fractional-order model better describes such system than integer order model. Although presented procedure implies ideal flexible structure model like cantilever beam, it is also suitable for application in active vibration control of real flexible structures, like aircraft wing, robotic manipulator, wind turbine blade, helicopter blade etc.

Key words: Active vibration control, System integration, System identification, Piezoelectric actuators.

1. Introduction

The rapid development of the industry, primarily aerospace and military industry as initiators of other industrial fields' development, requires application of new types of technologies. One of these new types of technologies is smart (intelligent, adaptive) structures. The main property of these structures is ability of adaptation to environmental conditions according to the design requirements by detecting and responding to disturbances. Smart structures are obtained by integration of actuators, sensors and controllers into conventional structures. The concept of a smart structure is important in active vibration control field. Due to external disturbances or influences of structural components, the appearance of unwanted vibration is unavoidable which present problem during development and exploitation of structures since these vibrations lead to decreased performances and catastrophic failures [1]. By using the concept of smart structures, unwanted vibrations can be reduced to the acceptable level or suppress completely. For this application, piezoelectric

materials are applied as actuators due its inverse piezoelectric effect. Also, due the direct piezoelectric effect, these materials can be applied as sensors.

The design process of a smart structure for active vibration control involves integration of actuators, sensors and controllers into a flexible structure. These components should be chosen and integrated in such way that obtained smart structure presents functional system. This paper describes mathematical modeling of smart structure with integrated piezoelectric actuators and sensors, procedure of selection and integration of piezoelectric actuators, sensors, signal conditioning system and piezoelectric actuator driver into cantilever aluminum beam in order to achieve desired performances for active vibration control. Also, design procedures of charge amplifier, required for signal conditioning from piezoelectric sensors as well as signal conditioning system for strain gauges are explained. The mathematical model is required to simulate a smart structure and selection of controller's parameter. In some cases, mathematical model varies from real structures due to unknown or imprecise parameters of materials and unmolded structural elements like adhesives between main structure and actuators and sensors. Also, dynamics of amplifiers and elements of signal conditioners are not involved into mathematical model, which can cause the phase shift between input and output. In order to avoid that, experimental identification of active vibration control system should be performed. According to the experimental data, integer order and fractional-order transfer functions are obtained in order to show if fractional-order model better describes such system than integer order model.

2. Mathematical model of flexible structures with integrated piezoelectric transducers

The specific enthalpy density of piezoelectric materials can be expressed as [2]

$$h=\frac{1}{2}\{\varepsilon\}^{\mathrm{T}}[C]\{\varepsilon\}-\{\varepsilon\}^{\mathrm{T}}[e]\{E\}-\frac{1}{2}\{E\}^{\mathrm{T}}[k]\{E\}, \tag{1}$$

where $[C]$ is the elastic stiffness matrix, $[e]$ is the piezoelectric constant matrix, $\{E\}$ is the electric field vector and $[k]$ is the permittivity matrix. Specific enthalpy density of elastic part of a structure can be obtained by setting piezoelectric of piezoelectric and permittivity constants to zero. Constitutive electromechanical equations in the stress-charge form are obtained as follows

$$\begin{aligned}\{\sigma\}&=\frac{\partial h}{\partial\{\varepsilon\}}=[C]\{\varepsilon\}-[e]^{\mathrm{T}}\{E\},\\ \{D\}&=-\frac{\partial h}{\partial\{E\}}=[e]\{\varepsilon\}+[k]\{E\},\end{aligned} \tag{2}$$

where $\{\sigma\}$ and $\{D\}$ represent the mechanical stress vector and the vector of electrical displacement respectively. Equations (2) can be written in the developed form [3]

$$\begin{Bmatrix}\sigma_1\\ \sigma_2\\ \sigma_3\\ \tau_{23}\\ \tau_{31}\\ \tau_{12}\end{Bmatrix}=\begin{bmatrix}C_{11}&C_{12}&C_{13}&0&0&C_{16}\\ C_{12}&C_{22}&C_{23}&0&0&C_{26}\\ C_{13}&C_{23}&C_{33}&0&0&C_{36}\\ 0&0&0&C_{44}&C_{45}&0\\ 0&0&0&C_{45}&C_{55}&0\\ C_{16}&C_{26}&C_{36}&0&0&C_{66}\end{bmatrix}\begin{Bmatrix}\varepsilon_1\\ \varepsilon_2\\ \varepsilon_3\\ \gamma_{23}\\ \gamma_{31}\\ \gamma_{12}\end{Bmatrix}-\begin{bmatrix}0&0&e_{31}\\ 0&0&e_{32}\\ 0&0&e_{33}\\ 0&e_{24}&0\\ e_{15}&0&0\\ 0&0&0\end{bmatrix}\begin{Bmatrix}E_1\\ E_2\\ E_3\end{Bmatrix} \tag{3}$$

$$\begin{Bmatrix} D_1 \\ D_2 \\ D_3 \end{Bmatrix} = \begin{bmatrix} 0 & 0 & 0 & 0 & e_{15} & 0 \\ 0 & 0 & 0 & e_{24} & 0 & 0 \\ e_{31} & e_{32} & e_{33} & 0 & 0 & 0 \end{bmatrix} \begin{Bmatrix} \varepsilon_1 \\ \varepsilon_2 \\ \varepsilon_3 \\ \gamma_{23} \\ \gamma_{31} \\ \gamma_{12} \end{Bmatrix} + \begin{bmatrix} k_{11} & 0 & 0 \\ 0 & k_{22} & 0 \\ 0 & 0 & k_{33} \end{bmatrix} \begin{Bmatrix} E_1 \\ E_2 \\ E_3 \end{Bmatrix} \tag{4}$$

After finite element discretization [3,4], it can be obtained following coupled electromechanical equation of motion in terms of nodal mechanical and electrical degrees of freedom:

$$\begin{aligned} [M]\{\ddot{u}\} + [C_\mathrm{d}]\{\dot{u}\} + [K_\mathrm{m}]\{u\} + [K_\mathrm{me}]_\mathrm{A}\{V\}_\mathrm{A} + [K_\mathrm{me}]_\mathrm{S}\{V\}_\mathrm{S} &= \{F_\mathrm{m}\} \\ [K_\mathrm{me}]_\mathrm{A}^\mathrm{T}\{u\} - [K_\mathrm{e}]_\mathrm{A}\{V\}_\mathrm{A} &= -[K_\mathrm{e}]_\mathrm{A}\{V\}_\mathrm{AA} \\ [K_\mathrm{me}]_\mathrm{S}^\mathrm{T}\{u\} - [K_\mathrm{e}]_\mathrm{S}\{V\}_\mathrm{S} &= 0, \end{aligned} \tag{5}$$

where $[M]$ presents the mass matrix, $[K_\mathrm{m}]$ is the elastic stiffness matrix, $[K_\mathrm{me}]_\mathrm{A}$ and $[K_\mathrm{me}]_\mathrm{S}$ are the piezoelectric stiffness matrices of the actuator and sensor respectively, $[K_\mathrm{e}]_\mathrm{A}$ and $[K_\mathrm{e}]_\mathrm{S}$ are dielectric stiffness matrices of the actuator and sensor respectively, $\{V\}_\mathrm{AA}$ is the vector of external voltage applied to actuators, $\{V\}_\mathrm{A}$ and $\{V\}_\mathrm{S}$ are voltages sensed by actuators and sensors respectively while $\{F_\mathrm{m}\}$ is the vector of external forces. From previous equation it can be obtained following equation of motion

$$[M]\{\ddot{u}\} + [C_\mathrm{d}]\{\dot{u}\} + [K^*]\{u\} = \{F_\mathrm{m}\} - [K_\mathrm{me}]_\mathrm{A}\{V\}_\mathrm{AA}, \tag{6}$$

where

$$[K^*] = [K_\mathrm{m}] + [K_\mathrm{me}]_\mathrm{A}[K_\mathrm{e}]_\mathrm{A}^{-1}[K_\mathrm{me}]_\mathrm{A}^\mathrm{T} + [K_\mathrm{me}]_\mathrm{S}[K_\mathrm{e}]_\mathrm{S}^{-1}[K_\mathrm{me}]_\mathrm{S}^\mathrm{T}, \tag{7}$$

From equation (5) it can be obtained the induced voltage from piezoelectric sensors:

$$\{V\}_\mathrm{S} = [K_\mathrm{e}]_\mathrm{S}^{-1}[K_\mathrm{me}]_\mathrm{S}^\mathrm{T}\{u\}. \tag{8}$$

Vector of the charge output of piezoelectric sensors is:

$$\{Q\}_\mathrm{S} = [K_\mathrm{e}]_\mathrm{S}\{V\}_\mathrm{S} = [K_\mathrm{me}]_\mathrm{S}^\mathrm{T}\{u\}. \tag{9}$$

For vibration analysis, the obtained model needs to be transformed into modal space, on following way

$$\{u\} \approx [\Psi]\{\eta\}, \tag{10}$$

where $[\Psi]$ represents the modal matrix and $\{\eta\}$ is the vector of modal coordinates. Substituting Equation (10) into Equation (6) leads to the following equation:

$$\{\ddot{\eta}\} + [\Lambda]\{\dot{\eta}\} + [\omega^2]\{\eta\} = [\Psi]^\mathrm{T}\{F_\mathrm{m}\} - [\Psi]^\mathrm{T}[K_\mathrm{me}]_\mathrm{A}\{V\}_\mathrm{AA}, \tag{11}$$

where $\left\lfloor \omega^2 \right\rfloor$ represents the diagonal matrix of the squares of the natural frequencies and $[\Lambda] = \underset{i=1,\ldots,r}{\text{diag}}\,(2\zeta_i\omega_i)$ represents the modal damping matrix in which ζ_i is the natural modal damping and r is the number of modes. In this case, sensors outputs can be written as

$$\begin{aligned} \{\dot{X}\} &= [A]\{X\} + [B]\{V\}_{\mathrm{AA}} + [\hat{B}]\{d\}, \\ \{Q\}_{\mathrm{S}} &= [K_{\mathrm{e}}]_{\mathrm{S}}\{V\}_{\mathrm{S}} = [K_{\mathrm{me}}]_{\mathrm{S}}^{\mathrm{T}}[\Psi]\{\eta\}. \end{aligned} \tag{12}$$

Equation (11) can be expressed in state-space form:

$$\{\dot{X}\} = [A]\{X\} + [B]\{\phi\}_{\mathrm{AA}} + [\hat{B}]\{d\}, \tag{13}$$

where

$$\{X\} = \begin{Bmatrix} \eta \\ \dot{\eta} \end{Bmatrix}, [A] = \begin{bmatrix} [0] & [\mathrm{I}] \\ -[\omega^2] & -[\Lambda] \end{bmatrix}, [B] = \begin{bmatrix} [0] \\ [\overline{B}] \end{bmatrix} = \begin{bmatrix} [0] \\ -[\Psi]^{\mathrm{T}}[K_{\mathrm{me}}]_{\mathrm{A}} \end{bmatrix}, [\hat{B}] = \begin{bmatrix} [0] \\ [\Psi]^{\mathrm{T}}\{F_{\mathrm{m}}\} \end{bmatrix} \tag{14}$$

present the state vector, the system matrix, the control matrix and disturbance matrices respectively, in which $[\mathrm{I}]$ and $[0]$ are the appropriately dimensioned identity and zero matrix respectively.

3. Piezoelectric actuators and high voltage amplifiers

Piezoelectric effect is found naturally in many crystal materials, such as quartz, tourmaline, topaz etc., but these materials are not suitable to be employed in active vibration control since weak piezoelectric properties. Instead, artificial materials, such as polyvinylidene fluoride (PVDF, thermoplastic fluoropolymer), and lead zirconate titanate (PZT, polycrystalline ceramic), are widely used since they can be processed to achieve significant piezoelectric properties. PZT ceramics possess strong electromechanical coupling, which make it suitable for piezoelectric actuator. On the other side, PVDF has great sensor characteristic. Both materials are relatively easy to produce.

For active vibration control of thin-walled structures, thin rectangular piezoelectric actuators and sensors are used. They thicknesses are below 1mm (around 0.2mm). Top and bottom sides of these piezoelectric patches are covered by electrodes. By applications of electric field across thickness, in plane deformations appear due piezoelectric constant e_{31} (Figure 1). Small thickness allows that less voltage is required for obtaining certain electric field. The piezoelectric constant e_{11} is larger than e_{31}, but much larger voltage across actuator's length is required for obtaining same electric field, which is not practical for real applications. Since PZT ceramic is very fragile, it is usually stacked between two layers of kapton or FR4 (glass-reinforced epoxy composite material). In order to increase actuating and sensing performances, piezoelectric fibers can be stacked into single layer composite, making so-called piezo-fiber reinforced composite (PFRC) actuator and sensor which provide high flexibility, durability and reliability [5].

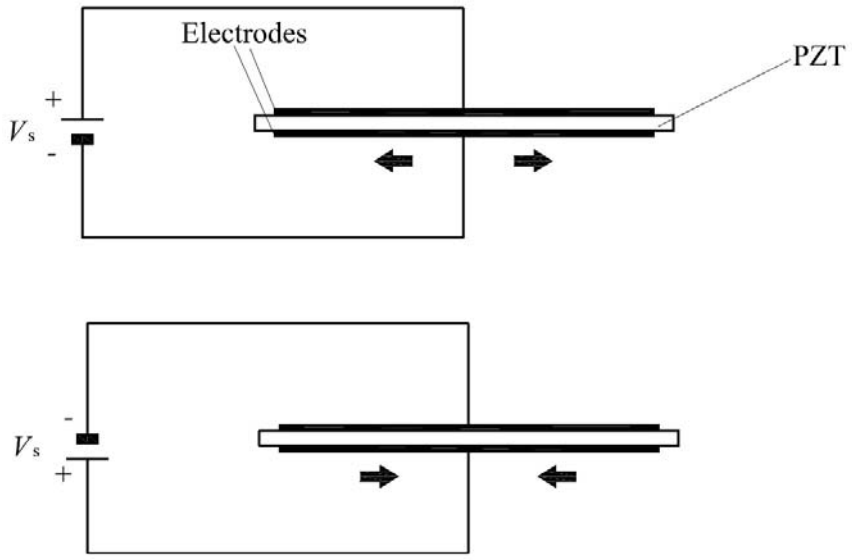

Fig 1. Work principle of piezoelectric actuators.

The allowable applied electric field of PZT materials is around 500–1000 V/mm. Since the thickness of the actuator is around 0.2 mm, maximum applied voltage is 100-200V in one direction, or ±100 V - ±200 V (200 V_{pp} – 400 V_{pp}). Maximum voltage from controllers is usually less than 10 V (for 32-byte microcontrollers such arm cortex-M and PIC32MX output voltage is 0 - 3.3 V). This means that control voltage needs to be linearly amplified. On the other side, piezoelectric actuators represents capacitive loads which actuations require certain amount of power, and current from controllers is very low. Maximum power consumption of piezoelectric actuators can be calculated as follows

$$P_{\max} = \pi C f V_{\text{pp}} V_{\max}, \tag{15}$$

where C presents the piezoelectric actuator capacitance, f is the driving frequency (Hz), V_{pp} is the peak-to-peak voltage and $V_{\max}$ is the maximum driving voltage.

There are many benchtop amplifiers available on market. They possess a wide range of frequencies (including DC) and voltages, which make them capable to drive wide range of piezoelectric actuators. Produced signal is clean with minimal noise and distortion. They are often chosen at the beginning of a development and in laboratory investigations. On the other side, price is very high, above 2000 euros. Also, they are often large, heavy and power hungry. Due to that, they are not suitable for industrial application. One of those benchtop amplifiers is presented in the Figure 2.

Fig 2. High voltage amplifier WMA-300 produced by Falco Systems.

In order to make amplifier according to operational requirements for certain regime with smaller dimensions, mass and power consumption which is suitable for usage in industrial application, integrated circuit style (single-chip) amplifiers are available on market.

In this paper, for active vibration control of the cantilever aluminum beam, the piezoelectric actuator, QP10W manufactured by Mide is chosen (Figure 3).

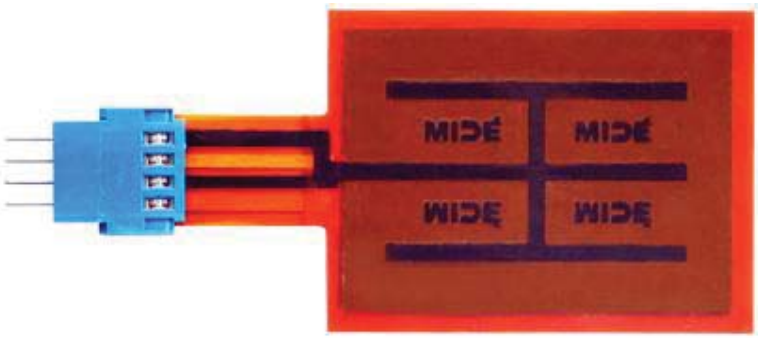

Fig 3. QP10W PZT actuator.

Capacitance of this actuator is 85nF, and maximum allowed voltage is ±200V ($400V_{pp}$ for sinusoidal load). Considering that 1st natural frequency of the beam is less than 30 Hz, maximum power of high voltage amplifier is less than 0.7 W. According to this requirement, single-chip amplifier DRV2700 produced by Texas Instruments is chosen. The DRV2700 presents a single-chip fully-differential amplifier available in QFN20 package (dimensions are 4.15mm x 4.15mm). The input signal can be either differential or single-ended and AC or DC coupled. Gains of the DRV2700 are 28.8dB, 34.8dB, 38.4dB and 40.7dB and they can be GPIO controlled. Maximum output voltage is ±100V (200 V_{pp}). Since operational amplifiers require supply voltage larger than output voltage, this device has integrated 105V boost which make it capable for low supply voltage (3V – 5.5V). Price of the DRV2700 is around 4$. According to the Figure 4, which presents characteristics of this amplifier, QP10W can be drive with maximum output voltage at the 400Hz. This makes the DRV2700 capable for required application.

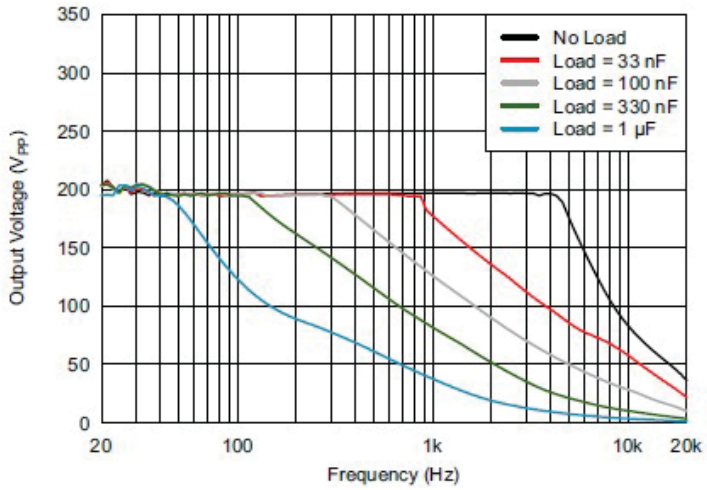

Fig 4. Driving characteristic of the DRV2700 high voltage amplifier (source: http://www.ti.com/lit/ds/slos861b/slos861b.pdf).

The evaluation kit DRV2700EVM produced by Texas Instruments, based on this amplifier, is also available with price of 149$ (Figure 5). This evaluation kit has integrated MSP430 controller and gains are setting with jumpers which allows for prototyping into already ecisting systems.

Fig 5. DRV2700EVM evaluation kit
(source: http://www.ti.com/lit/ug/slou403c/slou403c.pdf).

Other available single-chip amplifiers are those produced by Apex Microtechnology. These amplifiers are capable to drive at the higher voltages and the output power is up to 40W which make the them suitable for driving actuators with higher capacitances at the higher frequencies.

4. Sensors and signal conditioning

4.1 Strain gauge and full bridge configuration

Strain gauge presents device which measure strain according to the change of its resistance. In order to measure deformation of thin beams or plates, strain gauges are connected in a full Wheatstone bridge configuration. This configuration enables separation of normal and bending strain (only bending strain is measured), high output signal and excellent common mode rejection which is important for signal conditioning and temperature effects are well compensated. The Figure 6 presents the scheme of the full bridge Wheatstone configuration.

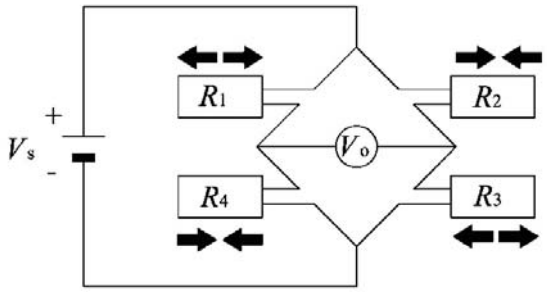

Fig 6. The scheme of the full bridge Wheatstone configuration.

The output from the full bridge Wheatstone configuration can be calculated as follows

$$V_{\mathrm{O}} = \left(\frac{R_3}{R_2 + R_3} - \frac{R_4}{R_1 + R_4} \right). \tag{16}$$

Since output voltage from full bridge in case of vibration is up to 10 mV, this signal needs to be amplified to several volts. In order to eliminate effects of common mode voltage, the instrumentation amplifier with high common-mode rejection, such AD623 produced by Analog devices, is selected. The Figure 7 presents circuits for data acquisition systems (the dual-supply case).

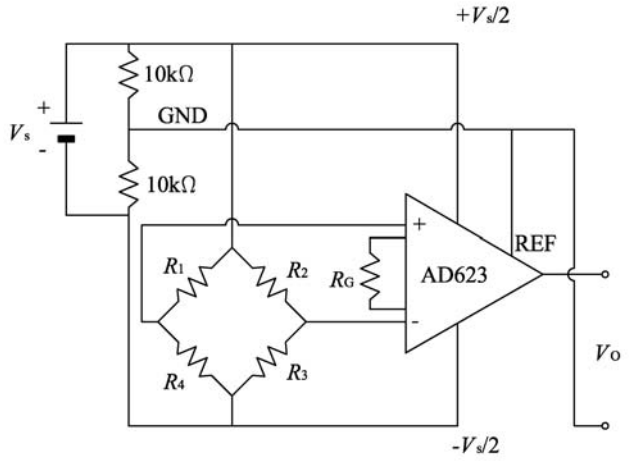

Fig 7. The circuit of data acquisition system for strain gauges; dual supply.

It is important that the strain gauges and instrumentation amplifier have the same supply. In that case, presented in the Figure 5, the common mode voltage is zero which allows that the output from amplifier swings between allowed minimum and maximum output of the amplifier ($-V_S/2+0.2\text{V} - V_S/2-0.5\text{V}$). The gain of the amplifier can be determined by resistance R_G on following:

$$A = 1 + \frac{100000}{R_G}. \tag{17}$$

It must be mentioned that microcontrollers do not allow negative voltage input respect to the ground, i.e. the negative voltage leads to the damage of microcontrollers. For this case, the circuit must be connected on the single-supply (Figure 8) thus the output will swing between $0.2\text{V} - V_S-0.5\text{V}$ and for balanced state, the output is $V_S/2$.

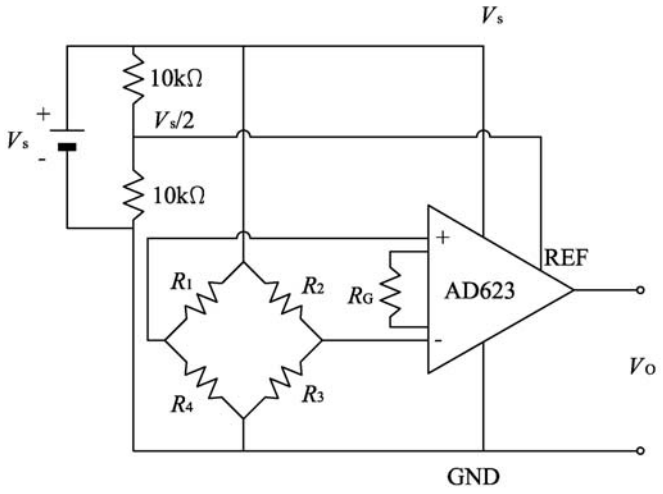

Fig 8. The circuit of data acquisition system for strain gauges; single supply.

4.2 Piezoelectric sensors

Due to direct piezoelectric effect, piezoelectric materials are capable to produce electric charge proportional to the deformation, which make them suitable for sensor applications. Piezoelectric actuators applied for active vibration control of thin-walled structures, explained in previous subsection, can be also used as sensors. Due to its elongation or compression along length, the electric charge appears at the electrodes. Piezoelectric sensor can be modeled as current source (Figure 9), where C_S and R_S present the capacitance and the resistance of the piezoelectric sensor, C_k is the capacitance of cables and R_M is the input resistance of a measure device.

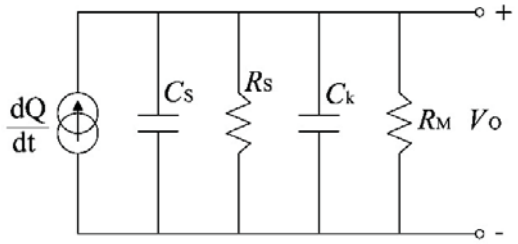

Fig 9. Piezoelectric sensor modeled as current source connected to a measure device.

The transfer function and the frequency response function relating the charge input and the voltage output are

$$H(s)=\frac{s}{(C_S+C_k)s+\frac{1}{R_S}+\frac{1}{R_M}},\quad G(j\omega)=\frac{j\omega}{j\omega(C_S+C_k)+\frac{1}{R_S}+\frac{1}{R_M}}, \tag{18}$$

Due to the finite resistance of measurement device, in case of measuring static deflection, the measured voltage of the piezoelectric sensor will always decay to zero [6]. Also, during vibration measurement, phase of output signal will be shifted. In order to perform pure strain measure and, in same time, avoid output signal dependence of measure device's resistance of as well as dependence of sensor's and cable's capacitances, charge amplifier is employed. The Figure 10 presents charge amplifier circuit and the Figure 11 presents equivalent circuit model of piezoelectric sensor connected to the charge amplifier, where real operational amplifier model is considered, in which R_i, R_O and R_f present the input, the output and the feedback resistance respectively, while C_i and C_f are the input and the feedback capacitance respectively.

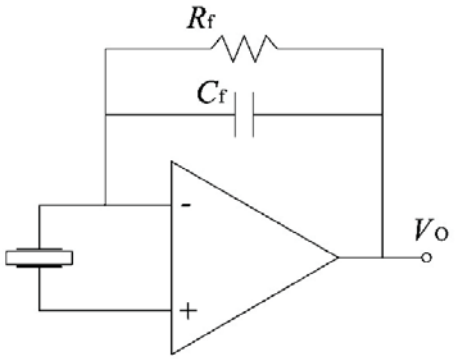

Fig 10. Charge amplifier circuit.

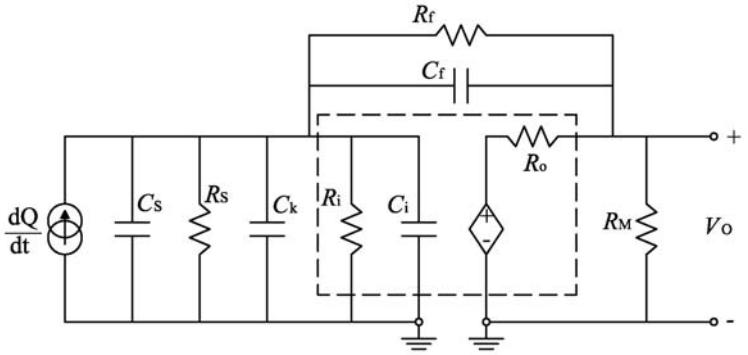

Fig 10. Equivalent circuit model of piezoelectric sensor connected to charge amplifier.

The frequency response function regarded to this circuit is:

$$G(j\omega)=\frac{V_{\mathrm{O}}(j\omega)}{\mathrm{Q}(j\omega)}=-\frac{j\omega(AG_{\mathrm{O}}-G_{\mathrm{f}})}{(G_{\mathrm{S}}+G_{\mathrm{k}}+G_{\mathrm{i}}+G_{\mathrm{f}})(G_{\mathrm{M}}+G_{\mathrm{f}}+G_{\mathrm{O}})+(AG_{\mathrm{O}}-G_{\mathrm{f}})G_{\mathrm{f}}}, \tag{19}$$

where A is the gain of an amplifier and $G_{\mathrm{S}}=\frac{1}{R_{\mathrm{S}}}+j\omega C_{\mathrm{S}}$, $G_{\mathrm{k}}=j\omega C_{\mathrm{k}}$, $G_{\mathrm{i}}=\frac{1}{R_{\mathrm{i}}}+j\omega C_{\mathrm{i}}$, $G_{\mathrm{f}}=\frac{1}{R_{\mathrm{f}}}+j\omega C_{\mathrm{f}}$, $G_{\mathrm{O}}=\frac{1}{R_{\mathrm{O}}}$, $G_{\mathrm{M}}=\frac{1}{R_{\mathrm{M}}}$. Considering that $R_{\mathrm{O}}<<R_{\mathrm{S}},R_{\mathrm{i}},R_{\mathrm{f}},R_{\mathrm{M}}$, the frequency response function can be written as follows

$$G(j\omega)=-\frac{j\omega A}{j\omega(C_{\mathrm{S}}+C_{\mathrm{k}}+C_{\mathrm{i}}+(A+1)C_{\mathrm{f}})+\frac{1}{R_{\mathrm{S}}}+\frac{1}{R_{\mathrm{i}}}+\frac{A+1}{R_{\mathrm{f}}}}. \tag{20}$$

Since gain of operational amplifier is larger than 10^5, and $R_{\mathrm{S}}\geq 10^{13}\Omega$, $R_{\mathrm{i}}\geq 10^{12}\Omega$ and $C_{\mathrm{f}}\geq C_{\mathrm{S}},C_{\mathrm{k}}$, previous equation has following form

$$H(j\omega) = -\frac{j\omega}{j\omega C_{\mathrm{f}} + \frac{1}{R_{\mathrm{f}}}}. \tag{21}$$

The cut-off frequency and the output voltage are

$$f_{\mathrm{c}} = \frac{1}{2\pi R_{\mathrm{f}} C_{\mathrm{f}}}, \quad V_{\mathrm{O}} = -\frac{\omega Q}{\sqrt{\frac{1}{R_{\mathrm{f}}^2} + \omega^2 C_{\mathrm{f}}^2}}. \tag{22}$$

In the frequency region larger than cut-off frequency, the output voltage can be reduced to the following form

$$V_{\mathrm{O}} = -\frac{Q}{C_{\mathrm{f}}}. \tag{23}$$

It can be concluded that previous equations are irrespective of the sensor's and measure device's resistance as well as cable's and sensor's capacitance and voltage output is proportional to the strain. Charge amplifier's gain and cut-off frequency can be controlled by choice of feedback capacitor and resistor. Feedback resistor provides DC stability to the circuit bleeds the charge of feedback capacitor at a low rate on order to prevent amplifier from drifting into saturation and also provides a DC bias path for the negative input.

4.3 Comparison between PZT sensor and strain gauges

In order to compare outputs from PZT sensor strain gauges the cantilever aluminum beam with integrated MIDE QP10W PZT patch and full bridge strain gauges (Figure 11) is employed. The resistance of strain gauge in balanced state is 120Ω. Dimensions of the beam are 240mm x 50mm x 1.5mm. Also, tip mass are added (two screws and nuts M6). The first natural frequency of the beam is 18.7Hz.

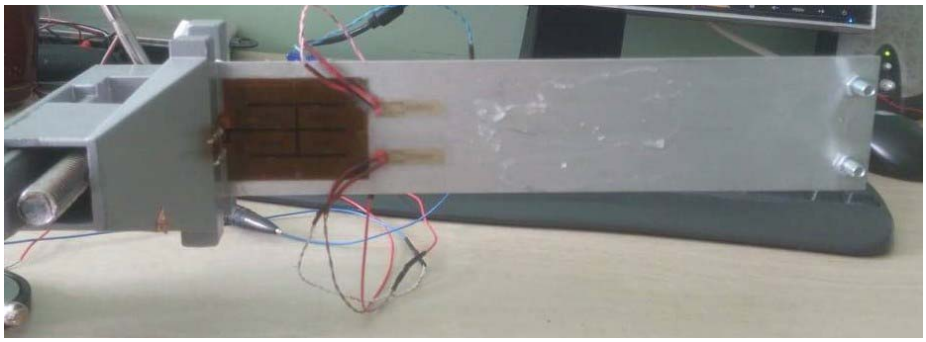

Fig 11. The cantilever aluminum beam with integrated MIDE QP10W PZT patch and full bridge strain gauges.

The operational amplifier LF347N is used for charge amplifier due to its low input bias current. The feedback capacitance and feedback resistance are selected to be 200nF and 20MΩ respectively. The circuit scheme is presented in Figure 12. Figure 13 shows the Bode plot of the charge amplifier.

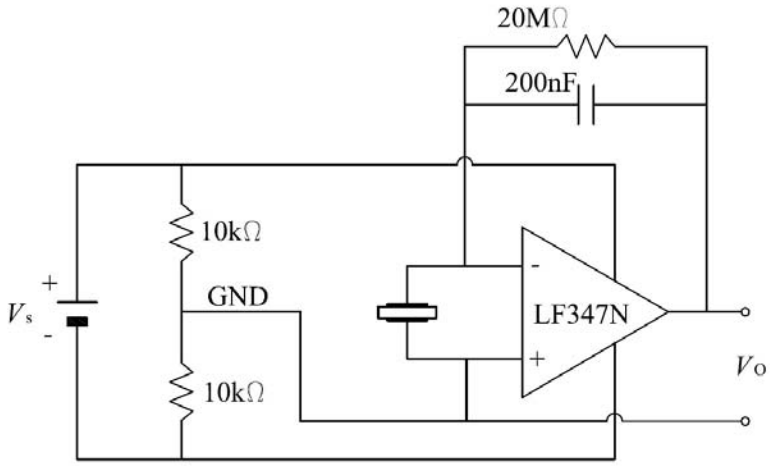

Fig 12. Circuit scheme of the charge amplifier.

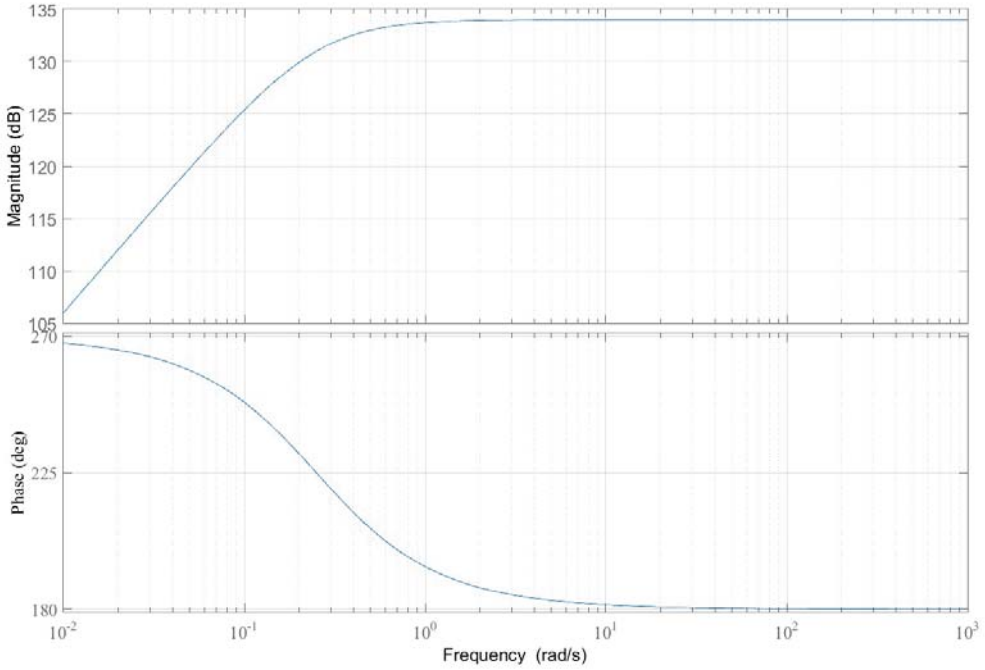

Fig 13. The Bode plot of the charge amplifier.

The Figure 14 illustrates outputs from PZT sensor and strain gauges under impulse load at the tip for two cases: the first case includes connecting the PZT sensor directly on the oscilloscope (Figure 14(a)) while the second case involves charge amplifier (Figure 14(b)).

From Fig 14(a) it can be concluded that that phase shift between outputs is presented, which is 10.7º. In second case, the phase shift is absent.

Next analysis is performed after putting additional mass at the tip which results in decreasing of the first natural frequency to 6.47Hz. Also, in this analysis, two cases are involved as in previous analysis. The Figure 15 presents outputs form the PZT sensor and strain gauges for these two cases. For directly measurement, the phase shift is 22.14º (Figure 15(a)) while for the second case, the phase shift is absent again (Figure 15(b)).

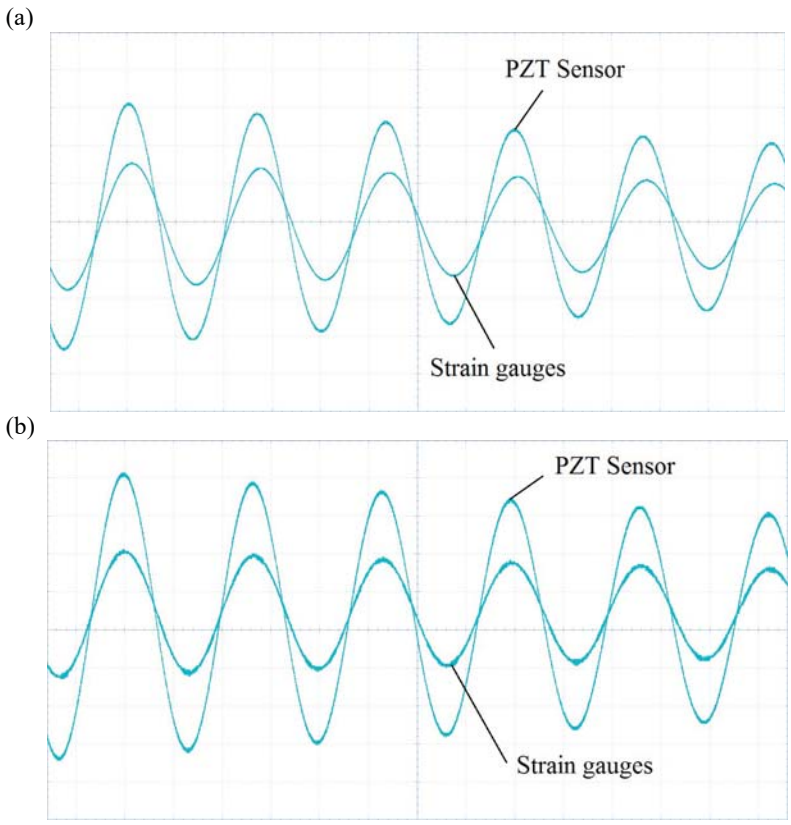

Fig 14. Comparison of outputs form PZT sensor and strain gauges under impulse load (1st natural frequency: 18.7Hz): a) the PZT sensor connected directly to the oscilloscope (horizontal line: 20ms/div, vertical line:5V/div for PZT sensor, 1V/div for Strain gauges), b) signal conditioning with the charge amplifier (horizontal line: 20ms/div, vertical line:1V/div for PZT sensor, 0.5V/div for Strain gauges).

From these analyses it can be concluded that the output signal from the PZT sensor is few time larger than from strain gauges, even for nonamplified signal of the PZT sensor. Also, piezoelectric sensor does not require external supply as well as connection to the various configurations in order to obtain desirable measurements which make them suitable for using in various working condition and for more complex structures. The sensitivity of the charge amplifier can be increased by decreasing the feedback capacitance, but in this case cut-off frequency will be shifted to right.

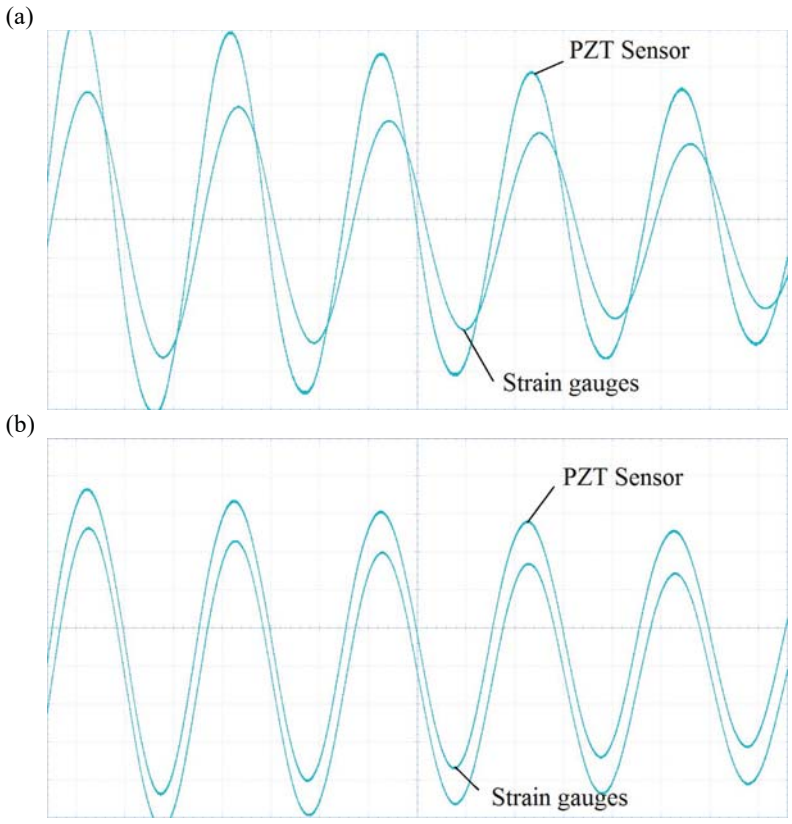

Fig 15. Comparison of outputs form PZT sensor and strain gauges under impulse load (1st natural frequency: 6.47Hz): a) the PZT sensor connected directly to the oscilloscope (horizontal line: 50ms/div, vertical line:5V/div for PZT sensor, 1V/div for Strain gauges), b) signal conditioning with the charge amplifier (horizontal line: 20ms/div, vertical line:2V/div for PZT sensor, 0.5V/div for Strain gauges).

5. System identification

Numerical analysis, such the finite element analysis, can provide the satisfactory dynamics behavior of smart structures, but some information can not be accurately determined [7]. This is especially expressed for determination of material damping properties, especially for large and complex structures. On the other side, model based controllers like LQR and H_∞ require as accurate as possible mathematical mode of a structure, hence determination of these material parameters is important task. In order to avoid this lack of numerical model, experimental identification of a structure is performed. In this subsection, experimental identification of smart cantilever aluminum beam (Figure 11) around the first resonant frequency will be presented. Consider the equation of forced vibration of the single-degree of freedom system:

$$m\ddot{x} + b\dot{x} + cx = F(t).. \tag{24}$$

Applying the Laplace transform of the equation (24), following transfer function can be obtained:

$$H(s) = \frac{X(s)}{F(s)} = \frac{1}{ms^2 + bs + c}. \tag{25}$$

Previous equation can be expressed in the parametric form:

$$H(s) = \frac{1}{a_1 s^2 + a_2 s + a_3}. \tag{26}$$

where a_1, a_2 and a_3 present parameters which will be determined through identification. For a sinusoidal input, the transfer function (26) can be expressed as frequency response function, which is defined as the transfer functions evaluated for $s = j\omega$:

$$G(j\omega) = \frac{1}{-a_1\omega^2 + a_2\omega j + a_3}. \tag{27}$$

The magnitude and the phase shift can be calculated as follows:

$$|G(j\omega)| = \sqrt{(\mathrm{Re}(G(j\omega)))^2 + (\mathrm{Im}(G(j\omega)))^2} = \frac{1}{\sqrt{(a_3 - a_1\omega^2)^2 + a_2^2\omega^2}}, \tag{28}$$

$$\angle G(j\omega) = \arctan\frac{\mathrm{Im}(G(j\omega))}{\mathrm{Re}(G(j\omega))} = -\arctan\frac{a_2\omega}{a_3 - a_1\omega^2}. \tag{29}$$

The identification procedure implies follows:

1. Excitation of the beam with sine signal through piezoelectric actuator on frequencies around the first resonant frequency,
2. Measuring the output from the sensor (strain gauges),
3. Calculating the ratio of the output and the input (magnitude) and phase shift between the output and the input,
4. Determination of parameters a_1, a_2 and a_3 through some optimization algorithm.

In this paper, the Particle swarm optimization (PSO) [8] will be employed for determination of these parameters. In this optimization procedure, parameters a_1, a_2 and a_3 will present coordinates of the particle. Optimization procedure implies minimization of following objective functions:

$$OBJ_1 = \sum_{i=1}^{n} \left(|G(j\omega)|_{\mathrm{exp}}(i) - |G(j\omega)|_{\mathrm{fit}}(i) \right)^2, \tag{30}$$

$$OBJ_2 = \sum_{i=1}^{n} \left(\angle G(j\omega)_{\text{exp}}(i) - \angle G(j\omega)_{\text{fit}}(i) \right)^2 , \tag{31}$$

where n presents the number of measured data points and subscripts exp and fit denote the experimental data and the data obtained from fitted function respectively. Following optimization problem can be transformed into single-objective problem as following:

$$OBJ = OBJ_1 + K \cdot OBJ_2 . \tag{32}$$

Since these two objective functions have not same order of magnitude, the scaling factor K is introduced. The experimental setup is presented in the Figure 16. Figure 17 illustrates the input and the output signal at the frequency 19Hz. Table 1 present the frequency, the peak-to-peak output voltage, the gain and the phase shift of each measurement. The peak-to-peak voltage from signal generator is set to be 1.75V.

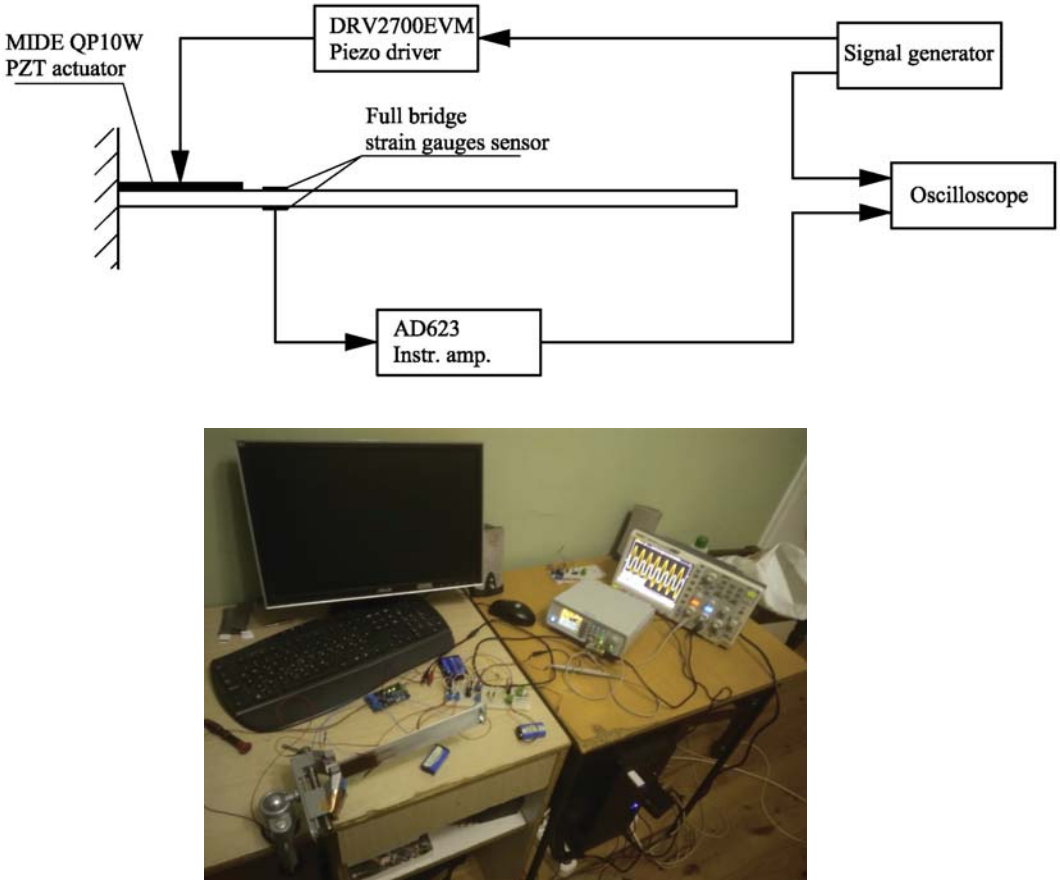

Fig 16. The experimental setup.

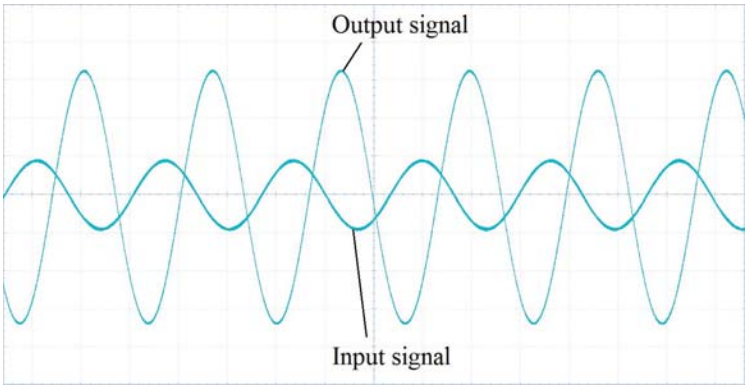

Fig 17. The input and the output signal at the 19Hz (horizontal line: 20ms/div, vertical line:1V/div).

i	Frequency (Hz)	Frequency (rad/s)	*V*pp out (V)	Magnitude	Magnitude (dB)	Phase shift (deg)
1	16	100.48	0.613	0.350	-9.112	-5.92
2	16.5	103.62	0.776	0.443	-7.064	-6.76
3	17	106.76	1	0.571	-4.861	-9.28
4	17.5	109.9	1.4	0.8	-1.938	-10.92
5	18	113.04	2.24	1.28	2.144	-16.84
6	18.3	114.924	3.55	2.028	6.144	-25.32
7	18.5	116.18	5.65	3.228	10.180	-41.468
8	18.7	117.436	8.6	4.914	13.829	-84.20
9	19	119.32	6.4	3.657	11.263	-132.58
10	19.5	122.46	3.48	1.988	5.971	-161.91
11	20	125.6	2.255	1.288	2.202	-169.968
12	20.5	128.74	1.7	0.971	-0.252	-174.22
13	21	131.88	1.39	0.794	-2.000	-176.01
14	21.5	135.02	1.19	0.68	-3.350	-177.26
15	22	138.16	1.05	0.6	-4.437	-177.96
16	22.5	141.3	0.95	0.543	-5.306	-178.71
17	23	144.44	0.875	0.5	-6.021	-179.32
18	23.5	147.58	0.81	0.463	-6.691	-179.79

Table 1. The frequency, the peak-to-peak output voltage, the magnitude and the phase shift of each measurement.

In the optimization algorithm, the phase shift was expressed in radians while the magnitude was expressed in absolute values. Also, it is determined that *OBJ*1 is around 27 times larger than *OBJ*2, thus the scaling factor *K* is set to be 27. The number of particles is 1000 and the number of iteration is 100. The following transfer function from optimization is obtained:

$$H(s)=\frac{1}{0.000567s^2+0.001727s+7.8668}\ , \tag{33}$$

and the objective function value is *OBJ*=2.279 (*OBJ*1=1.2946, *OBJ*2=0.03648).

Adhesives between piezoelectric actuator and the beam as well as between strain gauges and the beam possess viscoelastic properties. Viscoelastic nature of materials can be modeled by using fractional calculus [9]. The next step is obtaining fractional order transfer function from experimental data in order to show if fractional-order model better describes presented system than integer order model. The fractional-order transfer function of this system has following form [10]:

$$H_{\mathrm{FO}}(s)=\frac{1}{a_1s^2+a_2s^{\alpha}+a_3}\ , \tag{34}$$

and the frequency response function, related to the fractional-order transfer function, is

$$G_{\mathrm{FO}}(j\omega)=\frac{1}{a_1\omega^2+a_2\omega^{\alpha}\cos\frac{\alpha\pi}{2}+a_3+ja_2\omega^{\alpha}\sin\frac{\alpha\pi}{2}}\ . \tag{35}$$

Performing same optimization procedure (considering α as additional coordinate of the particle), following fractional-order transfer function is obtained:

$$H_{\mathrm{FO}}(s)=\frac{1}{0.0005632s^2+0.004623s^{0.8}+7.7543}, \tag{36}$$

and the objective function value is 2.2098 (*OBJ*1=1.2697, *OBJ*2=0.03482).

From this analysis it can be concluded that fractional-order model slightly better describes dynamics of the system compared to the integer order model. The Figure 18 presents the frequency response of the fractional-order model compared to the experimental data.

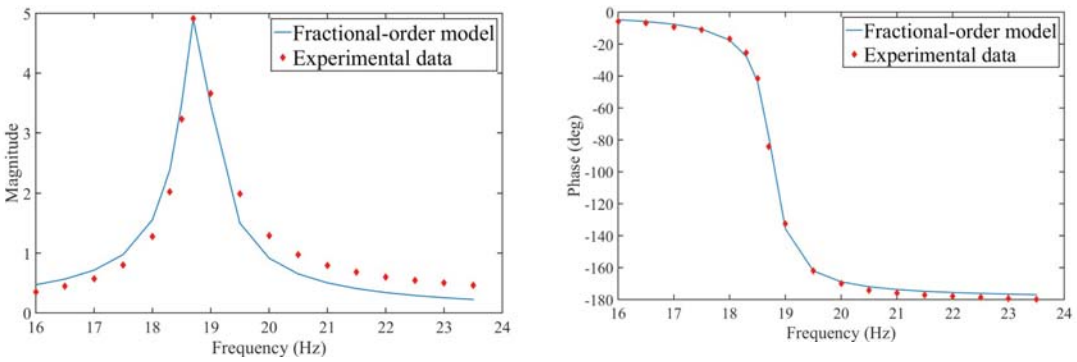

Fig 18. Frequency response of the fractional-order model compared to the experimental data.

6. Conclusions

This paper describes procedure of selection and integration of piezoelectric actuators, sensors, signal conditioning system and piezoelectric actuator driver into cantilever aluminum beam in order to achieve desired performances for active vibration control. The design procedures of charge amplifier, required for signal conditioning from piezoelectric sensors as well as signal conditioning system for strain gauges are detail explained along with the selection of proper amplifiers. Also, the experimental identification of smart structure based on cantilever aluminum beam is performed. According to the experimental data, integer order and fractional-order transfer functions are obtained. Transfer functions are parameterized and optimal values of these parameters are found by the Particle swarm optimization. Comparing objective functions, it is found that fractional-order model slightly better describes dynamics of the system compared to the integer order model.

References

[1] Worden, K., Bullough, W.,A., Haywood, J., *Smart Technologies*, Word Scientific, Singapore, 2003.
[2] Ballas, P.,G., *Piezoelectric Multilayer Beam Bending Actuators,* Heidelberg:Springer-Verlag, Berlin, 2007.
[3] Reddy, J.,N., *A simple higher-order theory for laminated composite plates*, Journal of Applied Mechanics, Vol. 51, 745-752, 1984.
[4] Zorić, N.,D., Simonović, M.,A., Mitrović, Z.,S., Stupar, S.,N., *Optimal vibration control of smart composite beams with optimal size and location of piezoelectric sensing and actuation*, Journal of Intelligent Material Systems and Structures, Vol. 24, 499-526, 2013.
[5] High, J.,W., Wilkie, W.,K., *Method of fabricating NASA-standard Macro-Fiber Composite piezoelectric actuators*, Technical Report NASA/TM-2003-212427, ARL-TR-2833. NASA Langley Research Center, Hampton, VA, USA, 2003.
[6] Ramanath, A.,K., Headings, L.,M., Dapino, M.,J*., Near DC force measurement using PVDF sensors*, Proceedings of SPIE 10602, Smart Structures and NDE for Industry 4.0, 106020M, 27 March 2018.
[7] Nestorovic, T., Trajkov, M., Patalong, M., *Identification of modal parameters for complex structures by experimental modal analysis approach*, Advances in Mechanical Engineering, Vol. 8, 1-16, 2016.
[8] Kennedy, J;, Eberhart, R.,C., *Particle swarm optimization*, Proceedings of the IEEE International Conference on Neural Networks, 1942-1948, 1995.
[9] Mainardi, F., *Fractional Calculus and Waves in Linear Viscoelasticity. An Introduction to Mathematical Models*, Imperial College Press, London, 2010.
[10] Muresan, C.,I., Folea, S., Birs, I.,R., Ionescu, C., *A novel fractional-order model and controller for vibration suppression in flexible smart beam*, Nonlinear Dynamics, Vol. 93, 525-541, 2018.